Environmental Science and Pollution Research (2023) 30:81403–81416
https://doi.org/10.1007/s11356-022-22791-6

ADVANCES IN WATER AND WASTEWATER TECHNOLOGIES FOR REMEDIATION OF CONTAMINANTS OF EMERGING CONCERN

ZnO-Zn_2TiO_4 heterostructure for highly efficient photocatalytic degradation of pharmaceuticals

Fatima Zahra Janani[1] · Habiba Khiar[1] · Nawal Taoufik[1] · Alaâeddine Elhalil[2] · M'hamed Sadiq[1] · Said Mansouri[3] · Noureddine Barka[1]

Received: 23 June 2022 / Accepted: 25 August 2022 / Published online: 31 August 2022

Abstract

In this study, ZnO-Zn_2TiO_4 (ZTM) material was prepared through a novel synthesis method based on a ultrasound-assisted polyol-mediated process followed by calcination at a different temperature. Physical features of the samples were studied by using various analysis techniques including XRD, FT-IR, SEM/EDX, pH_{PZC}, and UV–Vis DRS. Subsequently, the materials were employed as catalysts for the photocatalytic degradation of clofibric acid as a model pharmaceutical contaminant. The photocatalytic performance was evaluated under different conditions of calcination temperature, catalyst dosage, starting concentration, and initial pH of clofibric acid solution. The finding results revealed that hexagonal-tetragonal phases of ZnO-Zn_2TiO_4 calcined at 600 °C (ZTM-600) with an average crystallite size of 97.8 Å exhibited the best degradation efficiency (99%). The primary bands characteristic of ZnO and Zn_2TiO_4 were displayed by FT-IR analysis and the UV–visible DRS confirms the larger absorption capacity in UV–visible regions. The photogenerated electrons are the powerful reactive species involved in clofibric acid photodegradation process. This study shows a promising photocatalyst and provides new sight to rational design the facets of photocatalysis process for enhanced photocatalytic performances and effective wastewater treatment.

Keywords ZnO-Zn_2TiO_4 · Photodegradation · UV–visible light · Electrons charge transfer · Clofibric acid

Introduction

Recently, a consumption trend of pharmaceutical products has attracted considerable attention during the COVID-19 global pandemic, which leads industries to reorganize their strategies and adapt it to the current market requirements. These products include anti-inflammatories, antibiotics, and blood lipid regulators (Huma and Van Hullebusch 2020; Rosal et al. 2010; Taoufik et al. 2020).

Clofibric acid is a blood lipid regulator that is used all over the world (Huma and Van Hullebusch 2020; Rosal et al. 2010; Taoufik et al. 2020). It is classified as a bioactive metabolite of the clofibrate. This compound is considered as a one of the most frequently encountered major drug metabolite detected in the aquatic environment at ng/L-mg/L level (Wang et al. 2019; Ulvi et al. 2022). However, this molecule is recognized to be extremely resistant to biodegradation as well as other removal process like adsorption and hydrolysis, which remain its concentration at high level in the environment for a long time (Hemidouche et al. 2018; Dordio et al. 2009). Consequently, it is indispensable to provide a durable, eco-friendly, and sustainable technique to remove clofibric acid from wastewater. Many physical and chemical treatment processes have been investigated like coagulation/flocculation (Kooijman et al. 2020), adsorption (Zubair et al. 2012), and ozone-based advanced oxidation processes (Cai

Responsible Editor: George Z. Kyzas

✉ Noureddine Barka
barkanoureddine@yahoo.fr

[1] Sultan Moulay Slimane University of Beni Mellal, Multidisciplinary Research and Innovation Laboratory, FP Khouribga, BP.145, 2500, Khouribga, Morocco

[2] Laboratory of Process and Environmental Engineering, Higher School of Technology, Hassan II University of Casablanca, Casablanca, Morocco

[3] Materials Science Energy and Nanoengineering Department (MSN), VI Polytechnic University (UM6P), Lot 660-Hay Moulay Rachid, 43150 Benguerir, Mohammed, Morocco

et al. 2021; Li et al. 2019). However, these methods seem unsatisfactory.

Different from other methods, heterogeneous photocatalysis is a green technology that demonstrates its potential in the removal of different kind of pollutant from wastewater (Janani et al. 2021a). Moreover, the process is mild in response to inexhaustible irradiation as a source of energy, with a short processing cycle and high treatment efficiency. Based on these outstanding advantages, photocatalysis technology has become a promising means of pharmaceutical pollution control. This technique is designed to irradiate of appropriate semiconductors in a manner that generate active species with higher redox capacity. As of date, the development of semiconductors photocatalysts with low cost, high efficiency, and environmental friendliness is a big challenge for researchers. Hence, a wide variety of semiconductors has been synthesized for the photodegradation of pharmaceutical compounds.

TiO_2 is frequently used as efficient catalyst for clofibric acid degradation under ultraviolet light irradiation (Manassero et al. 2017; Harja et al. 2020; Rioja et al. 2014). However, it has a wide band gap, which allows to absorb only UV photons (Lu et al. 2020). As reported by Behineh et al. (2022), TiO_2 and Zn_2TiO_4 have a similarity in optical property. Despite this, the photocatalytic activities of Zn_2TiO_4 are higher than of TiO_2.

Zinc ortho titanate (Zn_2TiO_4) is present in ZnO-TiO_2 binary systems and is one of the most stable structures of these binary oxide system. It is a typical inverse spinel photocatalyst, particularly attractive thanks to its inexpensive, non-toxicity, outstanding stability, and optical properties in UV and near-visible light (Girish et al. 2018; Khatua et al. 2018; Lim et al. 2017; Purushan et al. 2018). Due to the high photocatalytic performances of ZnO and Zn_2TiO_4, many researches have been devoted to the coupling of both photocatalysts, in search of associated synergistic effect (Manchala et al. 2018; Behineh et al. 2022).

Wan et al. studied the photocatalytic degradation of acetone by using ZnO-Zn_2TiO_4 under UV irradiation. The results show a maximum degradation efficiency of 95% (Wan et al. 2010). In situ synthesis of ZnO/Zn_2TiO_4 nanocomposite from zinc hydroxide nitrate and evaluation of its photocatalytic performances by reactive black 5 dye was investigated by Pinto et al. (2018). Complete photodegradation of the pollutant achieved after 60 min under visible light irradiation. They showed that the photocatalytic activity of pure ZnO was considerably enhanced via the development of a ZnO/Zn_2TiO_4 heterostructure. Lim et al. proposed a fine synthesis method of multicore-shell ZnO@Zn_2TiO_4 spheres with a thin layer of carbon. The photocatalytic performance of this hybrid catalyst was evaluated by organic dye under solar light. About 93% degradation in 60 min was reached (Lim et al. 2017). However, the photocatalytic activity of the ZnO-Zn_2TiO_4 binary system is not evaluated under solar light. Therefore, the synthesis of this binary system without any modification, in the aim to improve their absorption capacity of the solar light region is a wise choice.

ZnO-Zn_2TiO_4 catalyst can be synthesized through various approaches including sol–gel, solid state, and hydrothermal. Nevertheless, there has been no report on the synthesis of ZnO-Zn_2TiO_4 with a significant absorption capacity in UV–visible light regions (simulated sun light). Consequently, it is important to develop a synthesis approach for the formation of ZnO-Zn_2TiO_4 heterostructure with a significant absorption capacity in UV–visible light regions, in order to conduct photodegradation with a low cost and ecology terms.

In the current research, an efficient photocatalyst for the degradation of clofibric acid as a model of pharmaceutical contaminants was reported. The prepared samples were characterized through various techniques including XRD, FT-IR, SEM, and DRS UV–visible analysis. In addition, the photocatalytic performance was compared with P25-TiO_2 under the same conditions and the detailed effects of important factors were studied.

Experimental

Chemical reagents

The starting reagents: zinc chloride ($Zn(Cl)_2{\cdot}6H_2O$, 99.8%), titanium isopropoxide (Ti(OiPr)4, 99.9%), urea ($CO(NH_2)_2$, 99.0%), ethylene glycol (C_6H_5OH, 99.5%), clofibric acid (C_2H_5OH, 99.5%), nitric acid (HNO_3, 37%), and sodium hydroxide (NaOH, 99.5%) were obtained from Sigma-Aldrich (Germany). TiO_2 Degussa P25 was employed as a reference photocatalyst. All the chemicals were employed without any modifications. Bidistilled water was used to prepare the solutions.

Synthesis of catalysts

The ZnO-Zn_2TiO_4 mixed oxides (ZTM) catalyst with total molar ratios of Zn/Ti of 4 was synthesized through ultrasound-assisted polyol-mediated process. Typically, appropriate amounts of $ZnCl_2$ and $Ti(OiPr)_4$ with the total concentration of metal cations set at 0.5 mol/L were dissolved in ethylene glycol as organic solvent and the mixture was stirred for 1 h at 90 °C. Then, urea solution (1 mol/L) was introduced to the above mixture. The mixture was latter sonicated at 90 °C for 10 min, and was kept under stirring at 120 °C for 20 h. The formed solid was subsequently filtered, washed with absolute ethanol, dried at 100 °C for 24 h, and then grounded to fine powder. Samples were calcined at different calcination temperature (400, 500, 600, and 800 °C). They were denoted ZTM-x, where x is the calcination temperature.

Characterization

The crystal phases of the obtained catalysts were analyzed through powder X-ray diffraction (XRD) on EMPYREAN, Configuration Reflexion–Transmission Spinner–MALVERN PANALYTICAL using Cu Kα radiation ($\lambda = 1.54A°$) with 45 kV acceleration voltage and 40 mA applied current. The XRD scans were performed in the 2θ region 5–80° with step size 0.06° (120 s/step), and the identification of the phases was performed by using HighScore software and Scherrer's formula was employed to determine crystallite size (Klubnuan et al. 2015).

$$D = \frac{K\lambda}{\beta\cos(\theta)} \tag{1}$$

where D is a crystallite size (nm), k is a constant (0.9), λ is the wavelength used (0.15406 nm), β is the peak width at half maximum in radian along (101) plane, and θ is a diffraction angle. Scanning electron microscopy (SEM) coupled to the energy dispersive X-ray spectroscopy (SEM/EDX) analysis was identified using a JSM-IT100-made EDS at an accelerating voltage of 30 kV. UV–Vis diffuse reflection spectroscopy (DRS) was performed to determinate the band gap energy of the photocatalyst by using a UV–visible-NIR spectroscopy: Perkin Elmer Lamda. The band gap value (E_g) of the catalyst was calculated from the UV-absorption spectra and the linear extrapolation of the Tauc plot of the Kubelka–Munk equation ($(F(R)\text{hv})^n$ vs. E_g), where, $F(R) = (1\text{-}R)^2/2R$ and R are the Kubelka–Munk and the relative diffuse reflectance, respectively.

where $n = 1/2$ or 2 are used for direct and indirect transitions, respectively.

The excitation of the electrons from the valance band to the conduction band of the ZTM-600 catalyst follows a direct transition. The valence band maximum EVB and the conduction band minimum ECB edges were determined according to the following equations:

$$E_{\text{CB}} = \chi - E_e - 0.5E_g \tag{2}$$

$$E_{\text{VB}} = E_{CB} + E_g \tag{3}$$

where the ECB, EVB, and E_g represent the conduction band potential, the valence band potential and the band gap, respectively. The E_e illustrates the free electron energy vs. hydrogen, which equal to 4.5 and the χ is the absolute electronegativity of the catalyst.

The point of zero charge (pH_{pzc}) was established to evaluate the surface charge characteristics of photocatalyst material, utilizing the method described by Noh and Schwarz (1989), the procedure is as explained below: A solution of NaCl (0.01 M) was prepared and subsequently partitioned into 6 solutions with pH varying from 2 to 12 adjusted using HCl and NaOH solutions (1 N). Following that, 0.05 g of catalyst was introduced to the solution. After 6 h of stirring, the pH of the mixture was determined. The pHpzc can be obtained at the point where the line of the final pH_f-$\text{pH}_i = f(\text{pH}_i)$ crosses the line of the starting pH.

Photocatalytic experiments

Photocatalytic experiments were conducted in a 1-L beaker irradiated on the top by 400 W halogen ($\lambda > 400$ nm: from 400 to 2000 nm) contained in a quartz water-jacketed to maintain the temperature of the reaction constant. In each run, 800 mL of 50 mg/L clofibric acid solution was incorporated into the beaker and, if necessary, the initial pH (pH_0) of the solution is adjusted by adding dilute nitric acid (HNO_3) or sodium hydroxide (NaOH) solutions. After that, 40 mg of catalyst (equivalent to 50 mg/L of catalyst dosage) was added to aqueous solution and the liquor was stirred for 30 min in the dark to achieve the adsorption/desorption equilibrium. Afterwards, the irradiation was initiated.

During photocatalytic tests, 3-mL aliquots were collected at predefined time intervals, filtered to remove the residual catalyst, and then analyzed at the wavelength of maximum absorption of 278 nm by using a METASH UV–Vis spectrophotometer. The photolysis test was performed following the same procedure without adding catalyst. In order to investigate the effect of operating parameters, catalyst dosage was varied from 12.5 to 100 mg/L, initial clofibric acid concentration from 25 to 100 mg/L, and the solution pH from 3.86 (natural) to 10.

A cycle of experiments was carried out under identical conditions in order to determine the stability and the reusability of the best catalyst. The suspensions were recovered by centrifugation, washed by bidistilled water to remove the residual clofibric acid, and dried at 100 °C for 24 h before using it in another photocatalytic test.

The photocatalytic performance of the catalysts was assessed by comparing the apparent reaction rate constant calculated from a pseudo-first-order kinetics expression as follow:

$$Ln(C_0/C_t) = k_{\text{ap}}t \tag{4}$$

where C_0 and C_t corresponds to the concentration of clofibric acid solution at $t = 0$ and at an irradiation time t, and k_{ap} represent the apparent reaction rate constant (min^{-1}).

Results and discussion

Characterization

X-ray diffraction (XRD) study

Figure 1 illustrates XRD patterns of the different samples with corresponding indexed phases. It can be observed

from the patterns that the XRD patterns of the samples calcined at 400 and 500 °C exhibit the main diffraction peaks reflected to ZnO (JCPDS file No. 36–1451). No reflection peaks characteristic for titanates appeared at these calcination temperatures, which confirm that the Ti-containing phases are amorphous or the metal is finely dispersed on ZnO phase. The only observed change in the diffractograms of the two catalysts is the development of the ZnO crystallinity in the material calcined at 500 °C. This phase is crystalized in hexagonal system, and the characteristic reflections appeared at approximately 2θ of 31.8°, 34.5°, 36.3°, 47.6°, 56.6°, 62.9°, 66.4°, 68°, and 69.1°, marked by reticular planes (100), (002), (101), (102), (110), (103), (200), (112), and (201), respectively. The sample calcined at 400 shows diffraction peaks corresponding to $Zn(OH)_2$ (JCPDS file No. 20–1436), these impurities could be attributed to the incomplete decomposition of $Zn(OH)_2$.

At calcination temperature of 600 °C, the characteristic reflections of Zn_2TiO_4 phase can be clearly observed. It is confirmed by the diffraction peaks located at 2θ = 29.85°, 35.15°, 42.65°, 53.4°, 56.5°, and 62°, related to the reflection planes (200) (220), (311), (400), (511), and (440). All these diffraction peaks are indexed with the tetragonal structure (P4mmm space group) (JCPDS file No. 86–0158). This phase can be resulted from the interaction between zinc oxide and titania which leads to a partial substituent of Ti^{4+} with Zn^{2+} (similar ionic radii = 0.61 Å and 0.60 Å). Crystallographically, Zn^{2+} can occupy octahedral sites of TiO_2, while Ti^{4+} cannot occupy tetrahedral sites of ZnO. Due to the fact that excess ZnO is maintained in the solid solution, Zn^{2+} can easy introduced in TiO_2 and the Zn_2TiO_4 can be obtained (Altalhi 2018). Moreover, it can be observed that the intensity of the peaks of ZnO decreased with the increase of calcination temperature to 600 °C, suggesting a partial transformation of ZnO to Zn_2TiO_4.

The catalyst calcined at 800 °C exhibits the characteristic XRD peaks of ZnO and tetragonal Zn_2TiO_4 as major phase. The diffraction peaks of Zn_2TiO_4 became more intensive and better pronounced. This result may be attributed to the high crystallinity of Zn_2TiO_4 at high temperatures (Perween and Ranjan 2017). On the other hand, the relative peak intensity near ~ 35° increased and simultaneously slightly shifted to

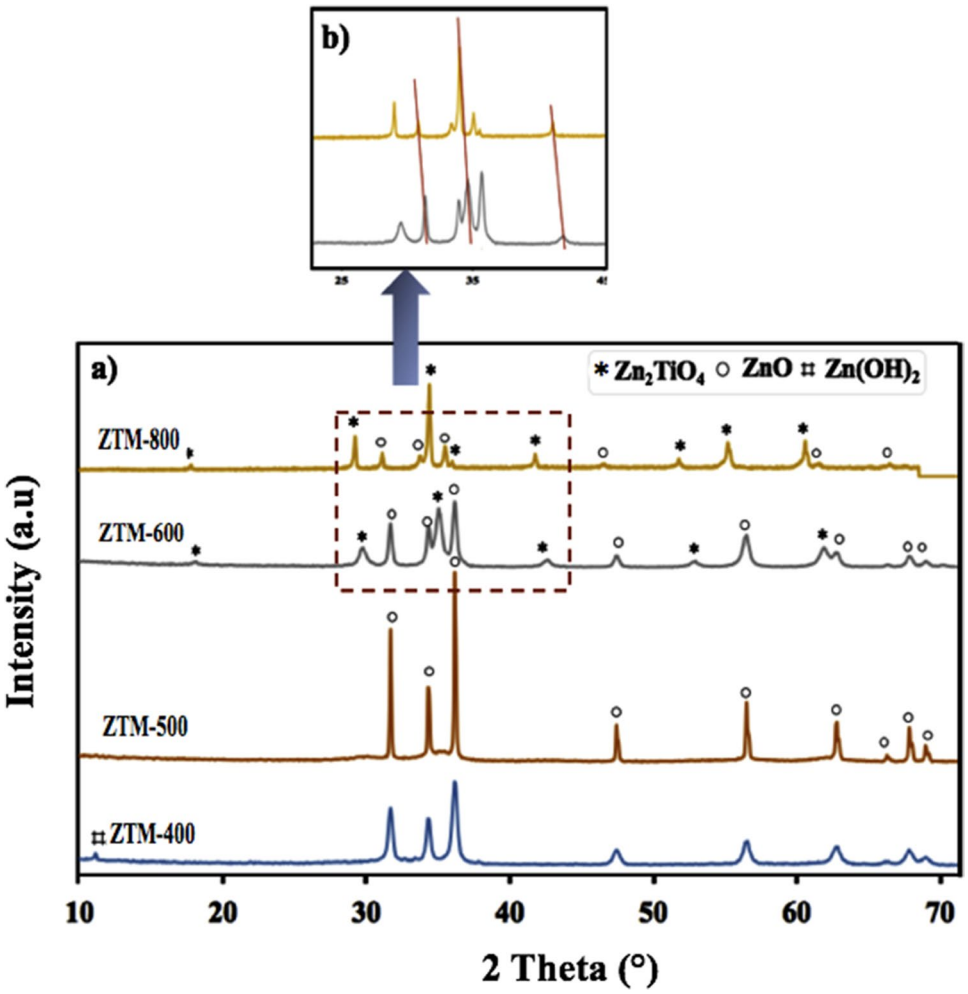

Fig. 1 XRD patterns of the calcined ZTM samples

lower angle as shown in Fig. 1.b). This result may be related to the crystallinity development of Zn_2TiO_4. Moreover, the obtained samples exhibit different crystallite size for each one 100, 485, 97.8, and 312.7 Å, which explain that this later is considerably dependent on the calcination process. It leads to the change of phase and structure from one temperature to another, which causes the change of crystallite size.

FT-IR spectra

The FT-IR spectra of as-synthesized catalysts are displayed in Fig. 2. The spectra of the samples calcined at 400 and 500 °C showed a broad band at 3600–3100 cm^{-1}, associated to stretching vibrations of hydroxyl groups of $Zn(OH)_2$ and/or some H_2O molecules absorbed from the air. The band shown at 1650 cm^{-1} can be reflected to bending vibrations of hydroxyl groups. These bands disappear in the spectra of the materials calcined at 600 and 800 °C. The metal–oxygen linkages vibrations were expressed in 1000–400 cm^{-1} region. As clearly observed from the spectrum, a weak band shown at around 442 cm^{-1} was originated from vibration of ZnO. This band was intensified by increasing calcination temperature, owing to the formation of crystalline wurtzite ZnO. The broad band observed at ~ 595 attributed to stretching vibrations in the octahedral TiO_6 group existing in the Zn_2TiO_4 phase (Ivanova et al. 2011).

SEM/EDX analysis

The surface morphology of the samples observed by SEM are shown in Fig. 3. It can be clearly observed a greatest difference in morphology of the obtained products with a relatively irregular contours of the agglomeration and structure. The formation of aggregation increased by increasing calcination temperature up to 600 °C, which can be resulted from the formation of ZnO/Zn_2TiO_4 heterostructure that was confirmed by XRD analysis. The surface of the calcined sample at 600 °C has more pores, which explain that the deshydroxylation of the precursors leads to the development of porous structure. The abundance particles size is less than 100 µm. It was increased by increasing calcination temperature from 400 to 600 °C and then decreased for calcination temperature of 800 °C. The grains were densely arranged and the particles were significantly distributed by calcination temperature rising, due to the sintering process of $ZnO\text{-}Zn_2TiO_4$ (Shih et al. 2009).

UV–Vis diffuse reflectance spectra

In order to understand the optical absorption properties of the photocatalyst, the UV–Vis DRS technique was performed and the obtained result is depicted in Fig. 4. It is clearly remarkable that the ZTM-600 photocatalyst shows

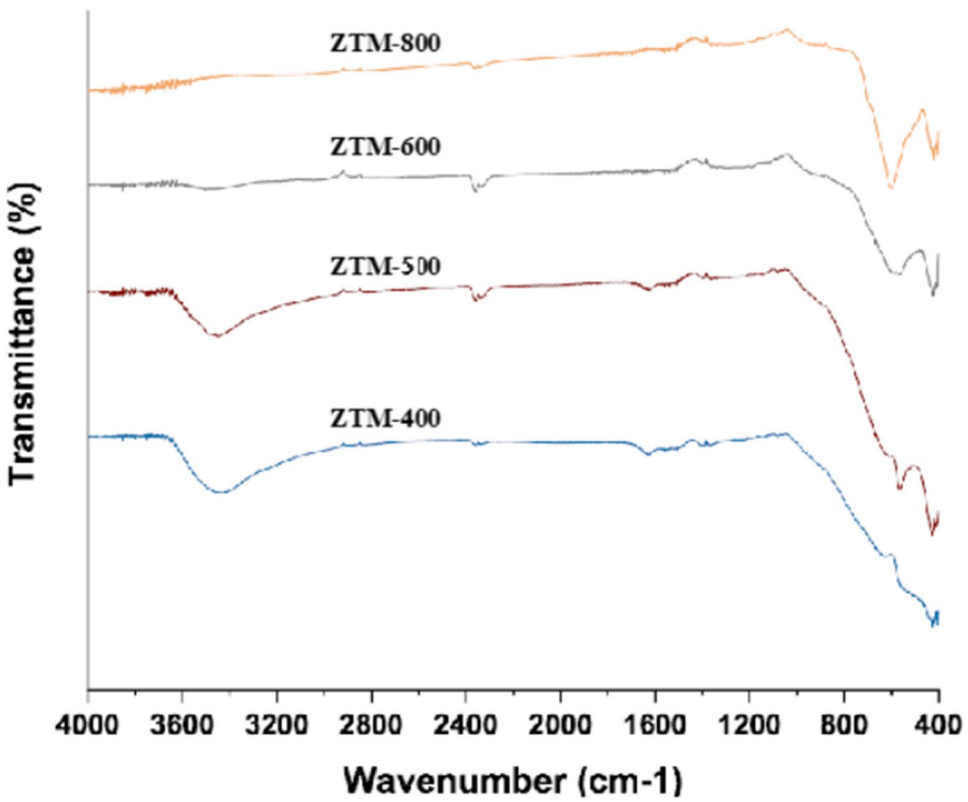

Fig. 2 FT-IR spectra of calcined ZTM samples

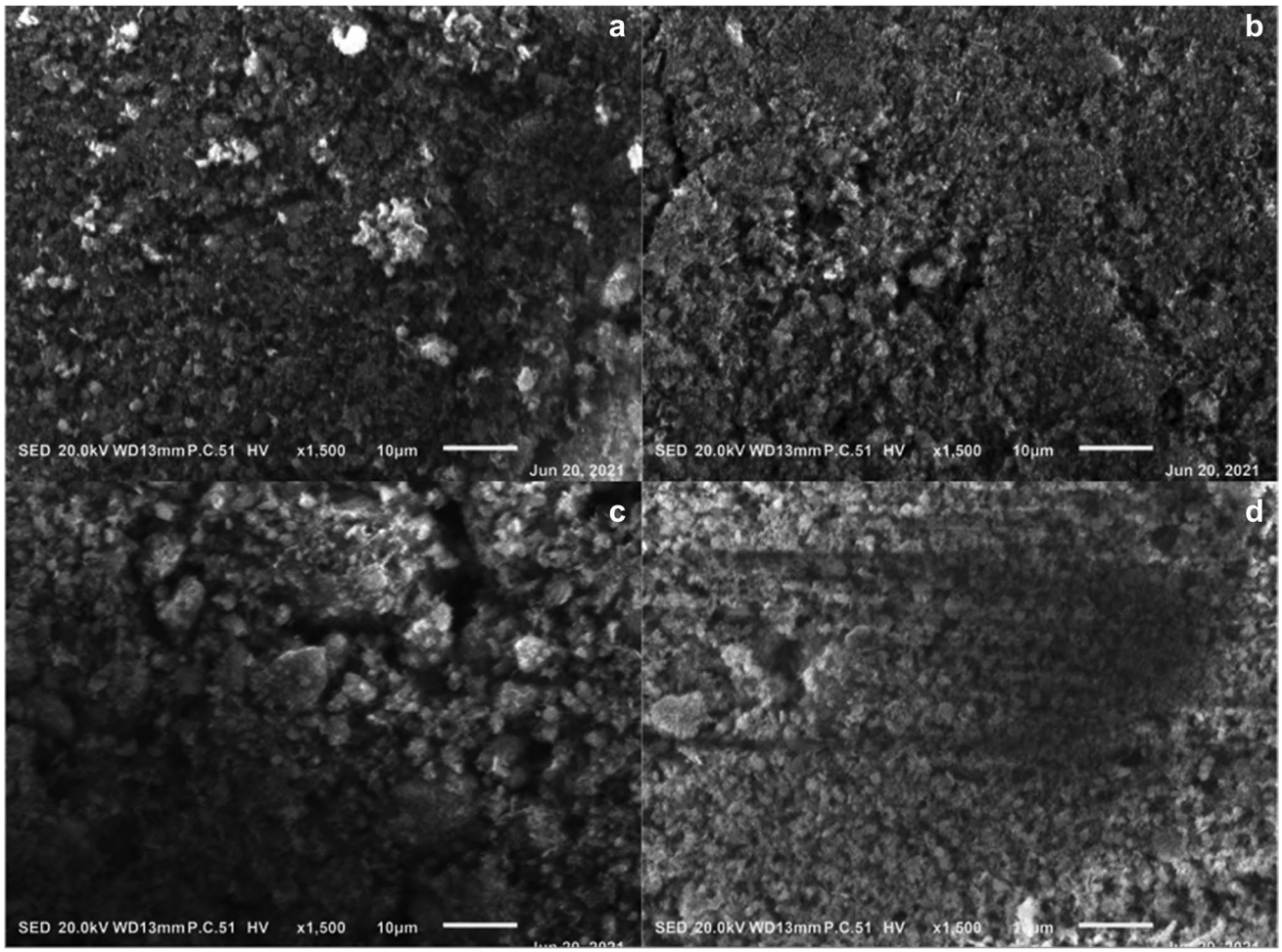

Fig. 3 SEM images of **a)** ZTM-400, **b)** ZTM-500, **c)** ZTM-600, and **d)** ZTM-800

absorption in both UV and visible regions with high absorbance at wavelengths less than 400, which correspond to a band gap energy of 2.89 eV calculated from the Tauc plot. The improved absorption capacity toward visible light of the catalyst may be related to the coupling of ZnO and Zn_2TiO_4. The smaller band gap of ZTM-600 indicates the easy transfer ability of electrons to conduction band, which produce more photogenerated charges. Consequently, the obtained catalyst could have efficient photocatalytic activity under UV and visible light irradiation.

pH_{PZC} determination

The point of zero charge (pH_{PZC}) is the parameter that corresponds to the pH for which the surface of the solid has a net zero charge. Its determination is necessary to estimate the acid–base behavior of the surface of the catalyst. This point is an important characteristic for surfaces, which represents the influence of the initial solution pH on the surface charge of catalysts. As depicted in Fig. 5, the pH_{PZC} of ZTM-600 was found to be 7. So, for pH > 7, the catalyst surface is negatively charged, while for pH < 7, the surface is positively charged. Therefore, the existence of positively charged ions on the catalyst surface in acidic medium, resulting the electrostatic attraction behavior, leading to an improvement of pollutant removal.

Photocatalytic degradation study

Effect of calcination temperature on the photocatalytic degradation

The kinetics of the adsorption/photodegradation of clofibric acid over different catalysts and compared with P-25 TiO_2 are shown in Fig. 6. It can be shown from the obtained data that the amounts of clofibric acid adsorbed in the dark are negligible. It is observed that After 90 min of irradiation time in the absence of the catalyst, only about 22% of clofibric acid was degraded and 30% after an exposure time of 180. This result suggests that the auto-oxidation of pollutant is not significant under light irradiation, which confirmed

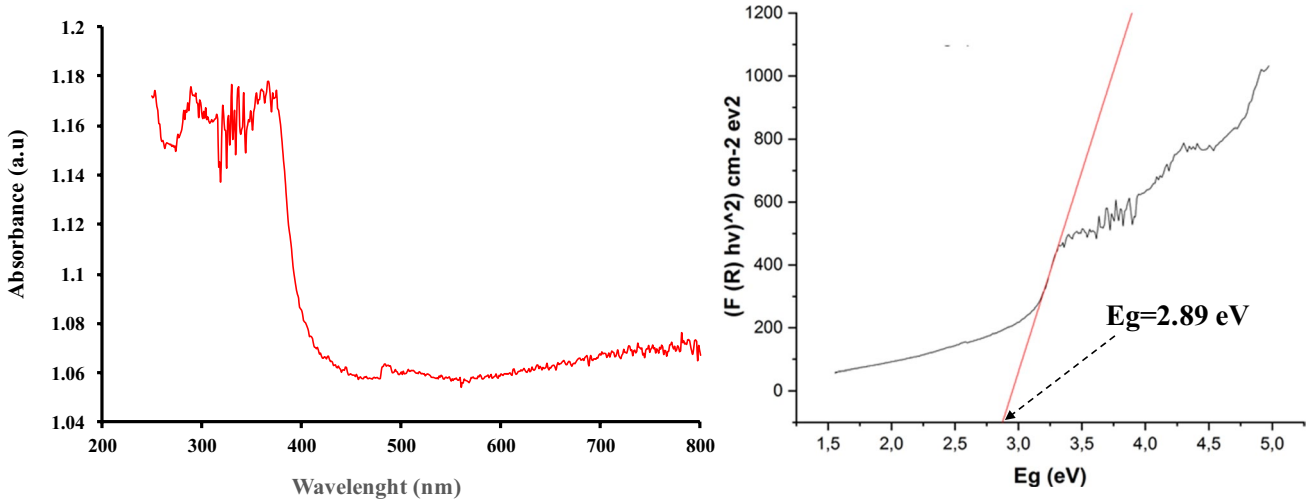

Fig. 4 UV–Vis DRS and band gap of ZTM-600 catalyst

Fig. 5 pH_{PZC} of ZTM-600

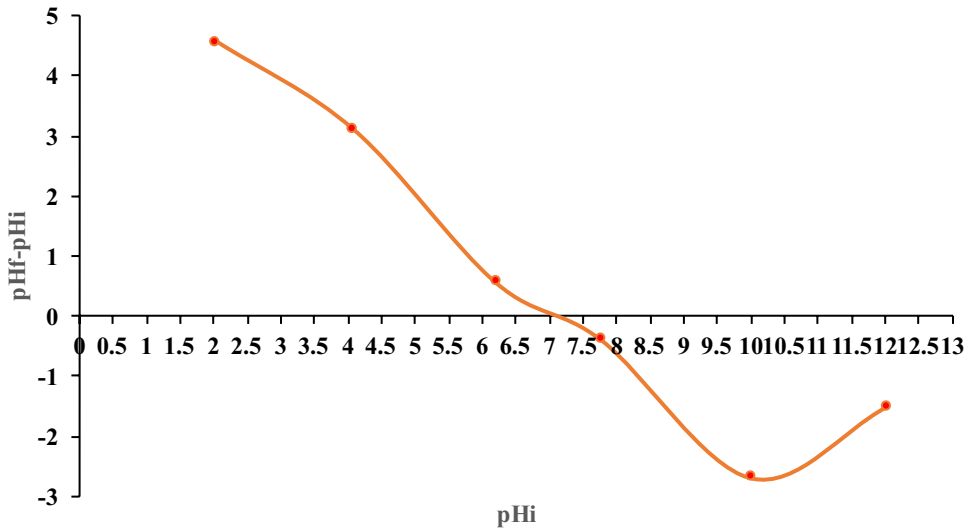

the importance of photocatalyst and light irradiation for a significant clofibric acid degradation. The obtained result is consistent with the result previously reported by Tolosana-Moranchel et al. (2019), which found a similar behavior. According to our result, the interference of the photolytic degradation with the photocatalytic degradation was neglected.

By addition of the catalysts, significant influence on the photocatalytic activity was observed. By increasing calcination temperature from 400 to 600 °C, an increase in the photodegradation rate was observed. The photocatalytic activity of the ZTM significantly improved with calcination temperature rising from 400 to 500 °C, assigned to the formation of ZnO oxide and its crystallization. At 600 °C of calcination temperature, the results display a highest photocatalytic performance which is mainly resulted to the synergistic effects between ZnO and Zn_2TiO_4 as the main constituents at this temperature confirmed by DRX. The photocatalytic activity drastically decreases by continuous calcination up to 800 °C. This can be due to the distortion of the heterostructure by the presence of some traces of ZnO phase and the formation of Zn_2TiO_4 as major phase, which considerably reduce the photogenerated charges separation behavior. As reported by Chai et al. (2019), the formation of Zn_2TiO_4 as major phase reduce the photocatalytic activities of the sample, this can be considered as the main reason of the decrease in the photocatalytic degradation efficiency. Consequently, it is reasonable that there is an optimal calcination temperature of the materials.

In the same order, the photocatalytic degradation of clofibric acid by all calcined samples was higher than that of P-25 titanium dioxide. It can be seen that after 90 min

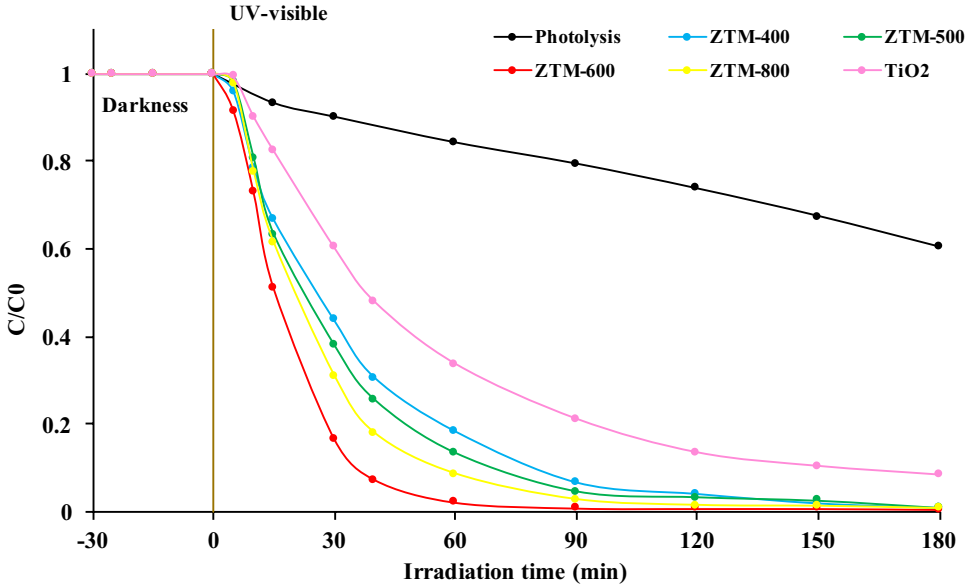

Fig. 6 Photocatalytic degradation of clofibric acid in the presence of synthesized catalysts compared with commercial Degussa P-25 (clofibric acid concentration: 50 mg/L; photocatalyst dosage: 50 mg/L; pH of the natural solution (~3.86))

of light exposure, ZTM samples calcined at 400, 500, 600, and 800 °C can decompose 93.2, 95.0, 99.1, and 95.3% of clofibric acid, respectively. However, the P25 nanoparticles reached only 78.8%. This suggests the superior UV–visible photocatalytic property of ZTM catalysts for the degradation of the target compound. This finding can be connected to different parameters, such as crystallinity degree, morphology, and electron–hole pair separation. In this sense, the small particles size and the irregular surface of the prepared photocatalyst that found by SEM analysis and the coupling of both semiconductors could deliver an adequate morphology to gives a better efficient photocatalytic efficiency under UV–visible light illumination. Owing to easy electron mobility across the interfacial heterostructure in the catalyst, which plays an important role by reducing the pathway from the site of photo-created electron–hole pair to the surface of catalyst. So, it is reasonable that the sample prepared through ultrasound-assisted polyol-mediated process, with a slightly lower particle size, can improve the photocatalytic degradation of the clofibric acid.

Similarly, various researches have studied the photocatalytic degradation of clofibric acid using numerous catalysts. Table 1 displayed that synthesized ZTM-600 by ultrasound-assisted polyol-mediated process holds excellent photocatalytic performances compared to other materials and methods reported in literature. Our study depicted that optimal process conditions 50 mg/L of ZTM-600 exhibited the maximum clofibric acid photodegradation efficiency of ~99.1% in 90 min. This is the first work reporting the clofibric acid degradation at high concentration.

Effect of initial clofibric acid concentration on the photocatalytic performances

Figure 7 depicts the kinetics of the photodegradation of clofibric acid at varied initial concentrations. The figure indicates a higher degradation efficiency at low concentration. However, increasing the clofibric acid concentration from 25 to 100 mg/L declined the extent of degradation from 99.8 to 97.1%. These results can be conducted to the clofibric acid molecules and the available actives sites ration, which was more important at higher initial concentration. Since the hydroxyl radical's lifetime is very short, they can only react near the site where they are formed (Barka et al. 2011). Thus, the number of degraded molecules to the number of created active species (·OH)

Table 1 Comparison of the photocatalytic activity of ZnO-Zn_2TiO_4 for clofibric acid with literature

Photocatalyst	Main conditions	Ratio (m/C_0)	Efficiency	Ref
g-C_3N_4/P25	C_0 = 2.0 mg/L; m = 0.5 g/L, pH = 5.3	r = 250	R = 85% after 30 min	Chen et al. 2017
TiO_2	C_0 = 1.5 mg/L; m = 1 g/L, pH = 5.9	r = 666.6	R = 85% after 130 min	Favier et al. 2019
Zn-La mixed oxide	C_0 = 20 mg/L; m = 500 mg/L, pH = natural	r = 25	R = 97% after 90 min	Sescu et al. 2020
ZnO-Zn_2TiO_4	C_0 = 50 mg/L; m = 50 mg/L, pH = 3.86	r = 1	R = 99.09% after 90 min	This work

increased with increasing initial concentration (Janani et al. 2021b). The competitive degradation behavior between clofibric acid molecules and its degradation intermediates also reduces the photocatalytic process, which could be important at high concentration of solution. Therefore, at a higher initial target pollutant concentration, a longer time is needed for its total degradation.

The initial rate of degradation was also affected by the initial concentration of clofibric acid. The initial rate decreased with increasing of initial clofibric acid concentration. This can be assigned to the fact that the photocatalyst dose and light irradiation flux remain constant, which with increasing of number of clofibric acid molecules, the photons penetration becomes more difficult to contact the catalyst surface. Indeed, a fewer number of active sites remain available for the generation of active species (hydroxyl radicals) needed for the photodegradation process. So, the clofibric acid degradation rate declined as the initial concentration increases due to the reduced production of hydroxyl radicals.

Effect of initial pH of clofibric acid solution

The pH value of the solution is an important parameter in the photocatalytic degradation process. It may affect significantly the photodegradation rate of clofibric acid in the presence of ZTM-600. As known, the pH_{PZC} of the catalyst and the pka values are two key factors. The pH_{PZC} of ZTM-600 is 7. At pH < 7, the ZTM-600 surface is positively charged and at pH > 7, it is negatively charged. The clofibric acid has pKa value of 3.18. Thus, the neutral clofibric acid form exists at pH below 3.18 and at pH above 3.18, the anionic form becomes predominant. As reported by Mestre et al. (2010), about 50 mol% of clofibric acid are in dissociated form at pH 3.6, and it was to be over 99 mol% dissociated at pH > 5.0. It can be noted from the Fig. 8 that the photodegradation efficiency clofibric acid at the initial pH value of 3.86 was 99.09 and the corresponding k_{app} was 0.0569 min^{-1}. When initial pH was increased to 7 and 10, the photodegradation performances declined to 90.8%, 0.0131 min^{-1} and 74.6%, 0.0083 min^{-1}, respectively. This indicated that the photocatalytic performances in natural acidic medium is higher than that at other solution pH values. These results might be assigned to the large amount of H^+ in acidic medium, which could be reduced by the photogenerated electrons, producing $H^{\cdot}$ radicals. The increase in the number of $H^{\cdot}$ radicals in the aqueous solution and on the surface of the catalyst increased considerably the photodegradation rate of clofibric acid (Kamranifar et al. 2021). They are also reacting with the adsorbed oxygen molecules, leading to the production of superoxide and hydroperoxide radicals, which contribute significantly in the photocatalytic degradation reaction. On the other hand, the degradation performance was decreased by increasing pH to 10. The excess of OH^- ions in the aqueous solution might be oxidized to $OH^{\cdot}$ radicals. However, the photodegradation rate decreased to 74.6%. This fact may be associated with the lower contribution of $OH^{\cdot}$ radicals in the photodegradation of clofibric acid as investigated by the quenching test of hydroxyl radicals. A similar result was found by Lin et al. (2021) for clofibric acid photocatalytic degradation by using g-C_3N_4/CeO_2. Consequently, the natural pH of clofibric acid was chosen an optimum value in furthers experiments.

Effect of photocatalyst dosage

The optimization of catalyst dosage is an important test to elucidate the relationship between the catalyst dosage and the photodegradation reaction as well as the photon

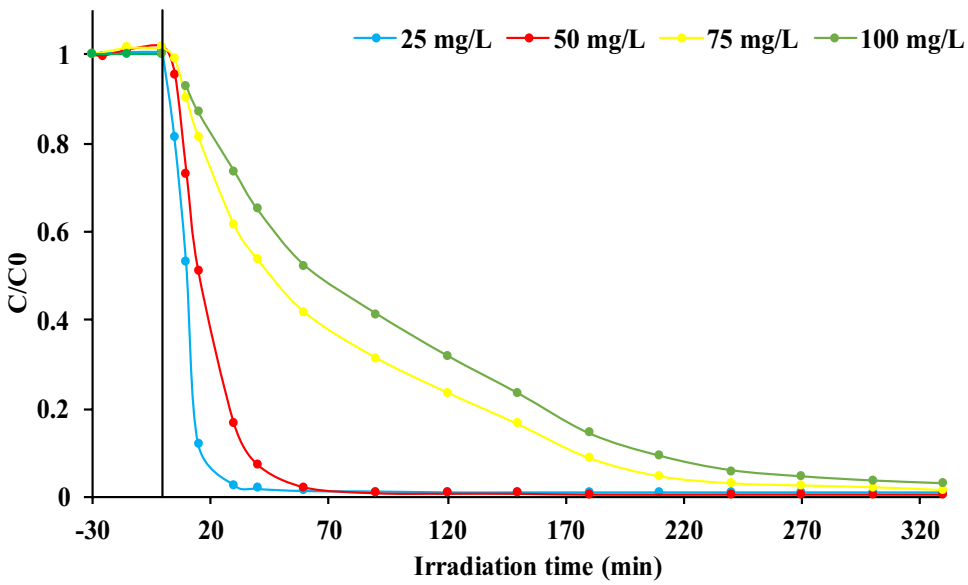

Fig. 7 Kinetics of clofibric acid photodegradation rate at different initial concentrations. Photocatalyst dosage: 50 mg/L; pH of the natural solution (~3.86)

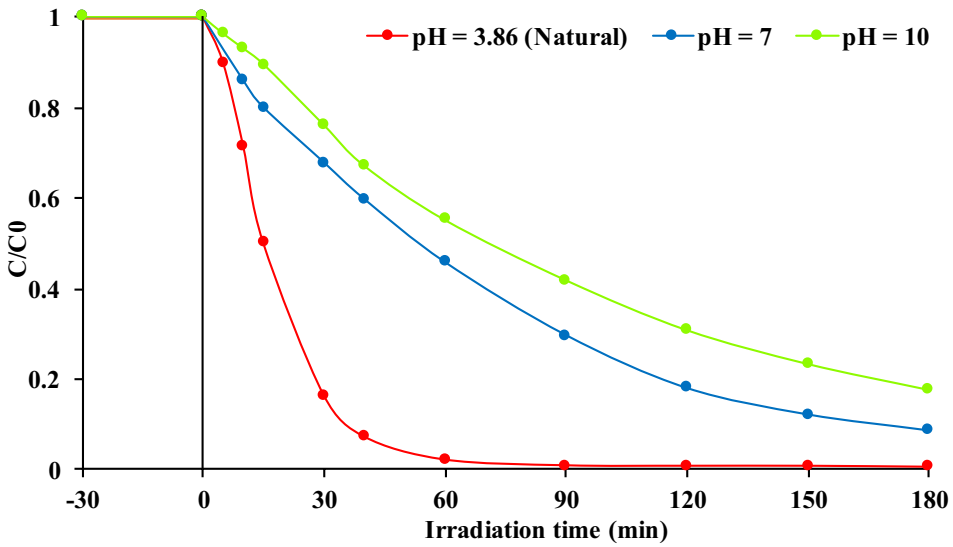

Fig. 8 Effect of initial pH of clofibric acid solution on its rate of degradation

absorption capacity. Results obtained from the variation of catalyst dosage are given in Fig. 9. The figure demonstrates that the photodegradation efficiency increased from 83.9 to 99.1% with rising catalyst dosage from 12.5 to 50 mg/L. Beyond this dose, as expected, the photodecomposition decreased with increasing of catalyst dose. This result is due to the aggregation or overlapping of semiconductor particles (Qourzal et al. 2012). Moreover, an inhibition of radiation penetration into the solution, due to the light scattering phenomenon resulting a low degradation efficiency. Similarly, Elhalil et al. (2019) demonstrated that the degradation of caffeine was declined by increasing Ag-ZnO-$La_2O_2CO_3$ photocatalysts amount. Consequently, the optimum catalyst dose of 50 mg/L was chosen in furthers experiments.

Photodegradation mechanism

The proposed photocatalytic degradation mechanism of clofibric acid utilizing ZTM-600 was illustrated in Fig. 10. Fundamentally, the photocatalytic process is mainly depend to a photo-induced active species such as electrons ($\bar{e}$), holes (h^+), hydroxyl radical ($^{\cdot}OH$), and superoxide radical ($O_2^{-\cdot}$). During the irradiation process, the electrons in the valence band move to conduction band and electrons-holes pairs are produced. The holes contribute to the production of hydroxyl radicals by oxidation of water molecules near the surface of catalyst. On the other side, the photo-induced electrons react with adsorbed oxygen molecules, leading to the formation of $^{\cdot}O_2$ superoxide radicals. The formed radicals can oxidize the clofibric acid present in the aqueous solution. The results

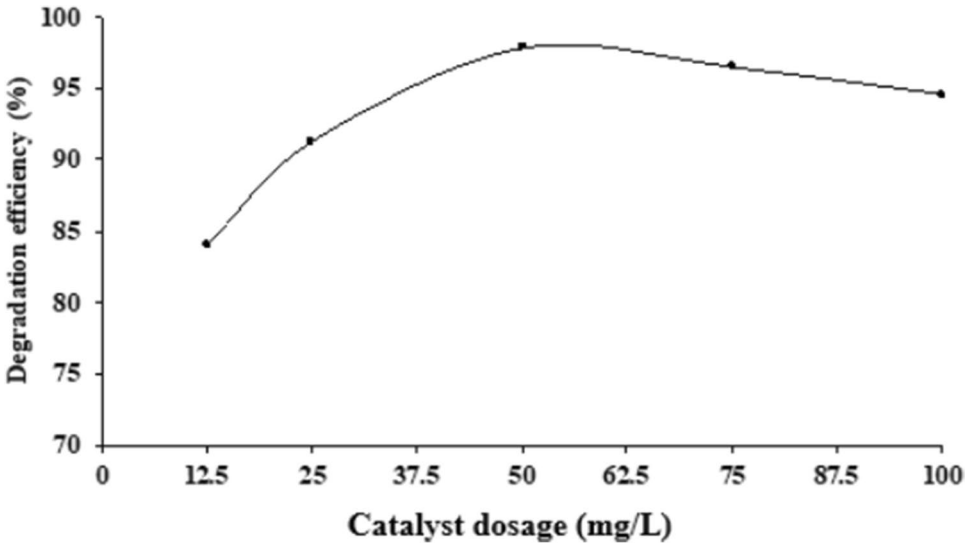

Fig. 9 Effect of ZTM-600 dosage on clofibric acid degradation efficiency

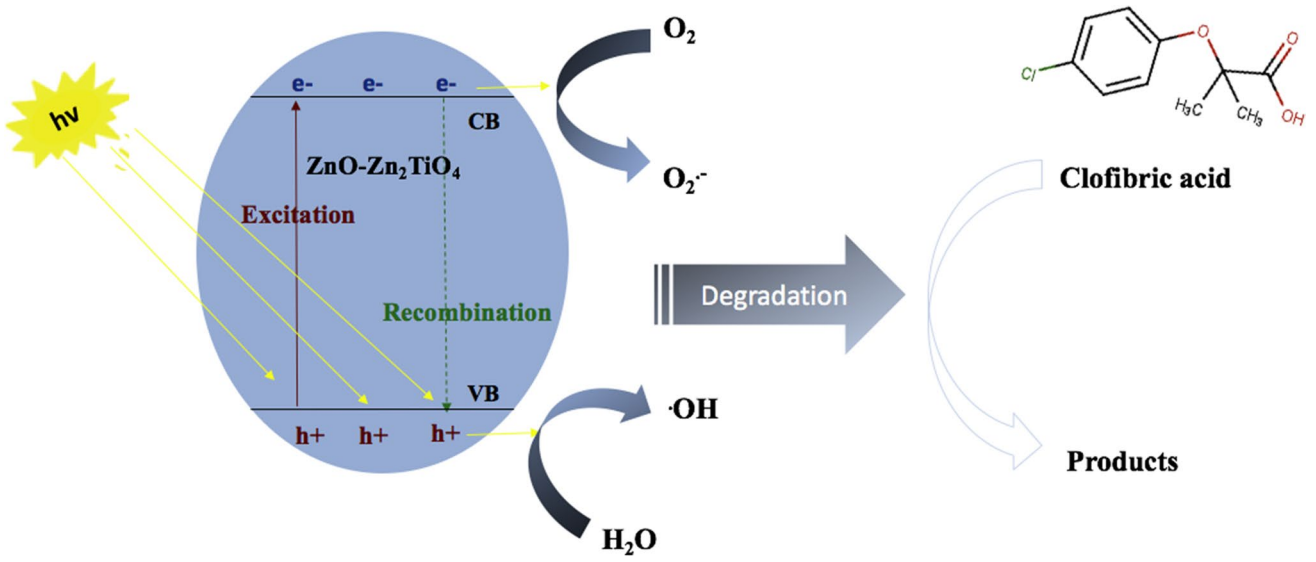

Fig. 10 Schematic illustration of the proposed photocatalytic degradation mechanism of clofibric acid by ZnO-Zn_2TiO_4 under UV-light

of radical quenching tests show that the photocatalytic degradation efficiency decreased slightly by adding ethanol and ascorbic acid, which achieved 46.2 and 58.4%, respectively. These results indicating that·OH and $O_2^{\cdot-}$ radicals are not the responsible species for clofibric acid. The degradation efficiency declined to 40% with the addition of EDTA, suggesting the slight contribution of the photogenerated holes for clofibric acid photodegradation. After the introduction of $AgNO_3$, the photodegradation efficiency apparently declined to 6.9%, which indicates that the electrons photo-induced are most likely the main ROS responsible in the photocatalytic degradation process of clofibric acid by ZTM-600.

The catalyst shows an enhanced absorption capacity in both ultraviolet and visible light regions, owing to their smaller band gap formation (2.89 eV). Therefore, the ZTM-600 requires less energy to generate electron–hole pairs, which leads to using a more photons resulting in an improvement photocatalytic activity. According to the calculated valence and conduction bands values, the E_{CB} of ZTM-600 is about 3.7 eV, which is more negative potential than the standard potential of the reduction of $O_2/O_2^{\cdot-}$ (−0.18 eV). The $O_2^{\cdot-}$ radicals formed by the reaction between the dissolved O_2 and the excited electrons on CB participated in the degradation reaction of clofibric acid. While, the holes generated on the VB of the catalyst cannot contribute to the production of·OH radicals, due to the lower positive VB potential (−0.54 eV) compared to that of $OH^-/{\cdot}OH$ and $H_2O/{\cdot}OH$, which have redox potential of (+1.99 eV vs. NHE) and (+2.44 eV vs. NHE), respectively. These results suggested that the few·OH radicals formed in the photocatalytic degradation process could be resulted from the photochemical reaction:

$$H_2O_2 + O_{2\cdot-} - \rightarrow .OH + OH^- + O_{2\cdot2-} \quad (5)$$

The photo-created holes contribute in the degradation reaction by direct oxidation of the organic molecule in the aqueous solution. Consequently, the photogenerated electrons are the powerful ROS in the photodegradation degradation. Thus, the h^+,·OH, $O_2^{\cdot-}$, take part in the photocatalytic process.

The photocatalytic efficiency could be reduced by increasing clofibric acid concentration or catalyst dose, which avoid the penetration of photons to catalyst surface. Therefore, the formation of photogenerated charges was reduced. The pH value of the clofibric acid also affected their catalytic degradation mechanism. It is more important in acidic medium than alkaline conditions. Indeed, the presence of H^+ in aqueous solution improves the catalytic photodegradation of clofibric acid. These protons were reduced by the generated electrons to H· radicals, which contribute to the formation of hydroxyl (·OH) and hyperoxide (HOO·) radicals. Consequently, the formation of the powerful active species in the photocatalytic process, considerably enhance the clofibric acid degradation. Ultimately, the principal reactions involved in the photocatalytic degradation of clofibric acid using ZTM-600 photocatalyst are outlined through the Eqs. (6) to (14) provided below:

$$ZnO - Zn_2TiO_4 + h\nu \rightarrow e^- + h^+ \quad (6)$$

$$O_2 + H^+ \rightarrow O_2^{\cdot-} \quad (7)$$

$$O_2^{\cdot-} + H^+ \rightarrow HOO^{\cdot} \quad (8)$$

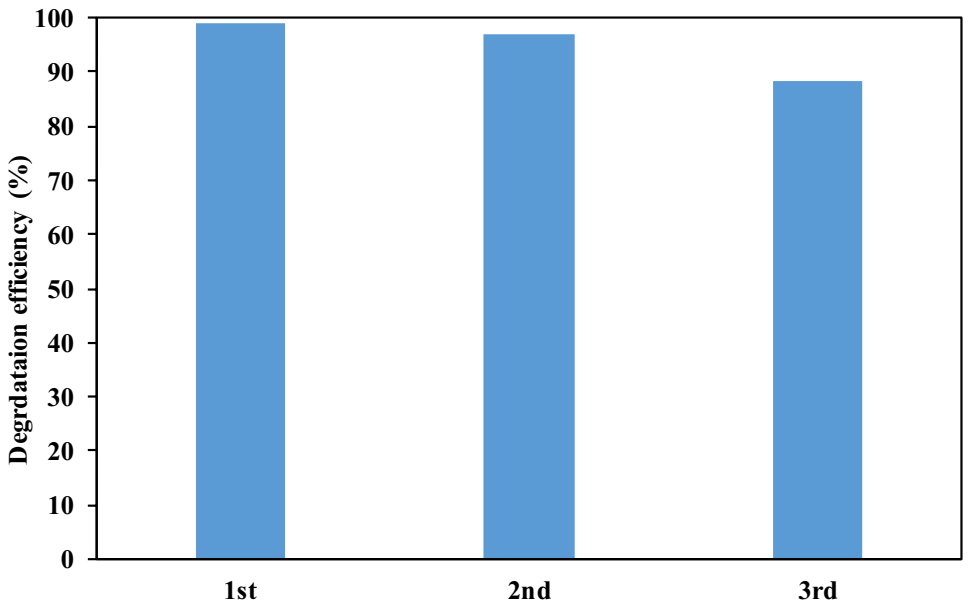

Fig. 11 Reusability runs for clofibric acid degradation over ZTM-600 under the same experiment conditions

$$HOO^{\cdot} + HOO^{\cdot} \rightarrow H_2O_2 + O_2 \quad (9)$$

$$H_2O_2 + O_2^{-} \rightarrow OH^{-} + OH^{\cdot} + O_2 \quad (10)$$

$$H_2O_2 + h\nu \rightarrow OH^{\cdot} \quad (11)$$

$$\text{Oxidationprocesses} : CA + h^{+}(VB) \rightarrow \text{degradedpollutant} \quad (12)$$

$$OH^{\cdot} + OH^{\cdot} \rightarrow H_2O_2 \quad (13)$$

$$CA + HO^{\cdot} \rightarrow CA(HO^{\cdot}) \rightarrow \text{intermediates} + HO^{\cdot} \rightarrow CO_2 + H_2O \quad (14)$$

Efficiency of the regenerated photocatalyst

The reusability and stability of the photocatalyst are therefore necessary for its practical applications. The recycling of ZnO-Zn_2TiO_4 was tested for many cycles under the same experimental conditions. From the results shown in Fig. 11, the photocatalytic decomposition of clofibric acid is maintained after 3 successive experimental runs, indicating that the ZnO-Zn_2TiO_4 photocatalyst exhibits a high photostability and reusability for organic compounds degradation. The finding suggest that the synthesized catalyst has a practical application potential in the removal of pharmaceuticals molecules.

Conclusion

A well ZnO-Zn_2TiO_4 heterostructure was synthesized through novel synthesis method based on ultrasound-assisted polyol-mediated process. Hexagonal-tetragonal phases were obtained after calcination of sample at 600 °C with abundance particles size less than 100 µm and with an efficient absorption capacity in both ultraviolet and visible regions. The high photocatalytic degradation performance of clofibric acid by ZTM-600 was assigned to the photo-induced electrons, which demonstrate their great reduction potential. Consequently, based on the findings, it is noticed that the photocatalysis process using ZnO-Zn_2TiO_4 catalyst was seem to be promising for the degradation of clofibric acid at pH natural of aqueous solution. The corresponding catalyst shows a highest photocatalytic performance activity under UV–visible illumination than those of other, reaching a high degradation efficiency of clofibric acid (50 mg/L) with a low catalyst dose of 50 mg/L. In conclusion, the excellent photocatalytic efficiency was attributed to synergetic effect between ZnO and Zn_2TiO_4, provided an appropriate charges separation on catalyst surface. The reusability tests indicate that the catalyst exhibits a high photostability the studied photocatalyst. This research could offer a facile route for the synthesis of effective and low-cost photocatalyst based on ZnO-Zn_2TiO_4 mixed oxides thus enable their application in environmental pollution control problems.

Author contribution All authors contributed to the study conception and design. Fatima Zahra Janani: performed the experiments; analyzed and interpreted the data, writing: original draft. Habiba Khiar: performed the experiments; analyzed and interpreted the data. Nawal Taoufik: analyzed and interpreted the data; data curation. Alaâeddine Elhalil: conceived and designed the experiments; analyzed and interpreted the data; data curation. Mhamed Sadiq: analyzed and interpreted the data; data curation. Said Mansouri: performed the experiments; analyzed and interpreted the data. Noureddine Barka: supervision, analyzed and interpreted the data; data curation, writing: review and editing, conceptualization, validation. All authors read and approved the final manuscript.

Data availability The datasets used and/or analyzed during the current study are available from the corresponding author on reasonable request.

Declarations

Competing interests The authors declare no competing interests.

References

Altalhi T (2018) Original strategy for facile synthesis of hybrid "ZnO-Zn2TiO4" nanotubes and antimicrobial activity. Mater Res Express 1–13.https://doi.org/10.1088/2053-1591/aad9d0

Barka N, Qourzal S, Assabbane A, Nounah A, Ait-Ichou Y (2011) Triphenylmethane dye, patent blue V, photocatalytic degradation on supported TiO2: kinetics, mineralization and reaction pathway. Chem Eng Comm 198:1233–1243. https://doi.org/10.1080/00986445.2010.525206

Behineh ES, Solaimany Nazar A, Farhadian M, Moghadam M (2022) Photocatalytic degradation of cefixime using visible light-driven Z-scheme ZnO nanorod/Zn2TiO4/GO heterostructure. J Environ Manage 316:115195. https://doi.org/10.1016/j.jenvman.2022.115195

Cai C, Duan X, Xie X, Kang S, Liao C, Dong J, Liu Y, Xiang S, Dionysiou DD (2021) Efficient degradation of clofibric acid by heterogeneous catalytic ozonation using CoFe2O4 catalyst in water. J Hazard Mater 410:124604. https://doi.org/10.1016/j.jhazmat.2020.124604

Chai Y, Li L, Lu J, Li D, Shen J, Zhang Y, Liang J, Wang X (2019) Germanium-substituted Zn_2TiO_4 solid solution photocatalyst for conversion of CO_2 into fuels. J Catal 371:144–152. https://doi.org/10.1016/j.jcat.2019.01.017

Chen P, Wang F, Zhang Q, Su Y, Shen L, Yao K, Chen ZF, Liu Y, Cai Z, Lv W, Liu G (2017) Photocatalytic degradation of clofibric acid by g-C3N4/P25 composites under simulated sunlight irradiation: the significant effects of reactive species. Chemosphere 172:193–200. https://doi.org/10.1016/j.chemosphere.2017.01.015

Dordio AV, Duarte C, Barreiros M, Carvalho Palace AJ, Pinto AP, Teixeira da Costa C (2009) Toxicity and removal efficiency of pharmaceutical metabolite clofibric acid by *Typha* spp. – potential use for phytoremediation? Bioresour Technol 100(2009):1156–1161. https://doi.org/10.1016/j.biortech.2008.08.034

Elhalil A, Elmoubarki R, Farnane M, Machrouhi A, Mahjoubi FZ, Sadiq M, Qourzal S, Abdennouri M, Barka N (2019) Novel Ag-ZnO-La2O2CO3 photocatalysts derived from the layered double hydroxide structure with excellent photocatalytic performance for the degradation of pharmaceutical compounds. J Sci: Adv Mater Devices 43:4–46. https://doi.org/10.1016/j.jsamd.2019.01.002

Favier L, Rusu L, Simion AI, Hlihor RM, Pacala ML, Augustyniak A (2019) efficient degradation of clofibric acid by heterogeneous photocatalytic oxidation process. Environ Eng Manage J 18:1683–1692

Girish KM, Prashantha SC, Nagabhushana H, Ravikumar CR, Nagaswarupa HP, Naik R, Premakumar HB, Umesh B (2018) Multifunctional Zn2TiO4:Sm3+ nanopowders: excellent performance as an electrochemical sensor and an UV photocatalyst. J Sci: Adv Mater Devices 3:151–160. https://doi.org/10.1016/j.jsamd.2018.02.001

Harja M, Sescu A, Favier L, Lutic D (2020) Doping titanium dioxide with palladiun for enhancing the photocatalytic decontamination and mineralization of a refractory water pollutant. Rev Chim 71(7):145–152. https://doi.org/10.37358/RC.20.7.8232

Hemidouche S, Favier L, Amrane A, Dabert P, Roux S, Sadaoui Z (2018) Successful biodegradation of a refractory pharmaceutical compound by an indigenous phenol-tolerant *Pseudomonas aeruginosa* strain. Water Air Soil Pollut 229:103. https://doi.org/10.1007/s11270-018-3684-6

Huma I, van Hullebusch ED (2020) Performance comparison of different types of constructed wetlands for the removal of pharmaceuticals and their transformation products: a review. Environ Sci Pollut Res 27:14342–14364. https://doi.org/10.1007/s11356-020-08165-w

Ivanova T, Harizanova A, Koutzarova T, Vertruyen B (2011) Preparation and characterization of ZnO–TiO2 films obtained by sol-gel method. J Non-Cryst Solids 357:2840–2845. https://doi.org/10.1016/j.jnoncrysol.2011.03.019

Janani FZ, Taoufik N, Khiar H, Boumya W, Elhalil A, Sadiq M, Puga AV, Barka N (2021a) Nanostructured layered double hydroxides based photocatalysts: insight on synthesis methods, application in water decontamination/splitting and antibacterial activity. Surf Interfaces 25:101263. https://doi.org/10.1016/j.surfin.2021.101263

Janani FZ, Khiar H, Taoufik N, Elhalil A, Sadiq M, Puga AV, Mansouri S, Barka N (2021b) ZnO-Al2O3-CeO2-Ce2O3 mixed metal oxides as a promising photocatalyst for methyl orange photocatalytic degradation. Mater Today Chem 21:100495. https://doi.org/10.1016/j.mtchem.2021.100495

Kamranifar M, Al-Musawi T, Amarzadeh M, Hosseinzadeh A, Nasseh N, Qutob M, Arghavan F (2021) Quick adsorption followed by lengthy photodegradation using FeNi3@SiO2@ZnO: a promising method for complete removal of penicillin G from wastewater. Journal of Water Process Engineering 40:101940. https://doi.org/10.1016/j.jwpe.2021.101940

Khatua L, Panda R, Nayak AK, Singh A, Sahoo PK, Pradhan D, Singh UP, Das SK (2018) Efficient UV photocatalytic dye decomposition activity with cost effective solid state reaction grown zinc orthotitanate (Zn2TiO4) nanoparticles. J Alloys Compd 764:895–900. https://doi.org/10.1016/j.jallcom.2018.06.126

Klubnuan S, Amornpitoksuk P, Suwanboon P (2015) Structural, optical and photocatalytic properties of MgO/ZnO nanocomposites prepared by a hydrothermal method. Mater Sci Semiconduc Proc 39:515–520. https://doi.org/10.1016/j.mssp.2015.05.049

Kooijman G, de Kreuk MK, Houtman C, van Lier JB (2020) Perspectives of coagulation/flocculation for the removal of pharmaceuticals from domestic wastewater: a critical view at experimental procedures. J Water Proc Eng 34:101161. https://doi.org/10.1016/j.jwpe.2020.101161

Li S, Tang S, Zhang J, Hao W, Chen W, Gu F, Hu Z, Li Z (2019) Advanced and green ozonation process for removal of clofibric acid in water system: preparation and mechanism analysis of efficient copper-substituted MCM-48. Sep Purif Technol 211:684–696. https://doi.org/10.1016/j.seppur.2018.10.031

Lim H-S, Lee J, Lee S, Kang YS, Sun YK, Suh K-D (2017) Walnut-like ZnO@Zn2TiO4 multicore-shell submicron spheres with a thin carbon layer: fine synthesis, facile structural control and solar light photocatalytic application. Acta Mater 122:287–297. https://doi.org/10.1016/j.actamat.2016.09.031

Lin H, Tang X, Wang J, Zeng Q, Chen H, Ren W, Sun J, Zhang H (2021) Enhanced visible-light photocatalysis of clofibric acid using graphitic carbon nitride modified by cerium oxide nanoparticles. J Hazard Mater 405:124204. https://doi.org/10.1016/j.jhazmat.2020.124204

Lu Z, Zhang K, Liu X, Shi Y (2020) Correction to: High efficiency inactivation of microalgae in ballast water by a new proposed dual-wave UV-photocatalysis system (UVA/UVC-TiO2). Environ Sci Pollut Res 27:8822. https://doi.org/10.1007/s11356-019-04268-1

Manassero A, Satuf ML, Alfano OM (2017) Photocatalytic degradation of an emerging pollutant by TiO2-coated glass rings: a kinetic study. Environ Sci Pollut Res 24:6031–6039. https://doi.org/10.1007/s11356-016-6855-2

Manchala S, Nagappagari LR, Venkatakrishnan SM, Shanker V (2018) Facile synthesis of noble-metal free polygonal Zn2TiO4 nanostructures for highly efficient photocatalytic hydrogen evolution under solar light irradiation. Int J Hydrogen Energy 43:13145–13157. https://doi.org/10.1016/j.ijhydene.2018.05.035

Mestre AS, Pinto ML, Nogueira JMF, Carvalho AP (2010) Effect of solution pH on the removal of clofibric acid by cork-based activated carbons. Carbon 48:972–980. https://doi.org/10.1016/j.carbon.2009.11.013

Noh JS, Schwarz JA (1989) Estimation of the point of zero charge of simple oxides by mass titration. J Colloid Interface Sci 130:157–164. https://doi.org/10.1016/0021-9797(89)90086-6

Perween S, Ranjan A (2017) Improved visible-light photocatalytic activity in ZnTiO3 nanopowder prepared by sol-electrospinning. Sol Energy Mater Sol Cells 163:148–156. https://doi.org/10.1016/j.solmat.2017.01.020

Pinto RB, Peralta-Zamora P, Wypych F (2018) Fabrication of ZnO-Zn2TiO4 nanocomposite from zinc hydroxide nitrate and its photocatalytic efficiency. J Photochem Photobiol A: Chem 353:46–52. https://doi.org/10.1016/j.jphotochem.2017.11.008

Purushan GK, Sarma S, Chatterjee A, Kumar GK, Suresh Kumar NV (2018) Effect of Fe doping on structural and transport properties of inverse spinel Zn2TiO4. Inter J Chem Tech Research 11:58–64. https://doi.org/10.20902/IJCTR.2018.110806

Qourzal S, Barka N, Belmouden M, Abaamrane A, Alahiane S, Elouardi M, Assabbane A, Ait-Ichou Y (2012) Heterogeneous photocatalytic degradation of 4-nitrophenol on suspended titania surface in a dynamic photoreactor. Fresenius Environ Bull 21(7):1972–1981

Rioja N, Benguria P, Peñas FJ, Zorita S (2014) Competitive removal of pharmaceuticals from environmental waters by adsorption and photocatalytic degradation. Environ Sci Pollut Res 21:11168–11177. https://doi.org/10.1007/s11356-014-2593-5

Rosal R, Rodea-Palomares I, Boltes K, Fernández-Piñas F, Leganés F, Soledad G, Alice P (2010) Ecotoxicity assessment of lipid regulators in water and biologically treated wastewater using three aquatic organisms. Environ Sci Pollut Res 17:135–144. https://doi.org/10.1007/s11356-009-0137-1

Sescu AM, Harja M, Favier L, Berthou LO, De Castro CG, Puia A, Lutic D (2020) Zn/La mixed oxides prepared by coprecipitation: synthesis, characterization and photocatalytic studies. Materials 13:4916. https://doi.org/10.3390/ma13214916

Shih CH, Li WM, Lin MM, Hsiao CY, Hung KT (2009) Low-temperature sintered Zn2TiO4:TiO2 with near-zero temperature coefficient of resonant frequency at microwave frequency. J Alloys Compd 485:408–412. https://doi.org/10.1016/j.jallcom.2009.05.153

Taoufik N, Boumya W, Janani FZ, Elhalil A, Mahjoubi FZ, Barka N (2020) Removal of pharmaceutical pollutants: a systematic mapping study review. J Environ Chem Eng 8(5):104251. https://doi.org/10.1016/j.jece.2020.104251

Tolosana-Moranchel A, Manassero A, Satuf ML, Alfano OM, Casas JA, Bahamonde A (2019) TiO_2-rGO photocatalytic degradation of an emerging pollutant: kinetic modelling and determination of intrinsic kinetic parameters. J Environ Chem Eng 7:103406. https://doi.org/10.1016/j.jece.2019.103406

Ulvi A, Aydın S, Aydın ME (2022) Fate of selected pharmaceuticals in hospital and municipal wastewater effluent: occurrence, removal, and environmental risk assessment. Environ Sci Pollut Res. https://doi.org/10.1007/s11356-022-21131-y

Wan L, Li X, Qu Z, Shi Y, Li H, Zhao Q, Chen G (2010) Facile synthesis of ZnO/Zn2TiO4 core/shell nanowires for photocatalytic oxidation of acetone. J Hazard Mater 184:864–868. https://doi.org/10.1016/j.jhazmat.2010.08.004

Wang L, Fang J, Zhang X, Xu X, Kong X, Wu Z, Hua Z, Ren Z, Guo K (2019) Feasibility of the solar/chlorine treatment for lipid regulator degradation in simulated and real waters: the oxidation chemistry and affecting factors. Chemosphere 226:123–131. https://doi.org/10.1016/j.chemosphere.2019.03.102

Zubair H, Jaewoo J, Sung HJ (2012) Adsorptive removal of naproxen and clofibric acid from water using metal-organic frameworks. J Hazard Mater 209–210:151–157. https://doi.org/10.1016/j.jhazmat.2012.01.005